*J. Fluid Mech.* (1998), *vol.* 377, *pp.* 169–187. Printed in the United Kingdom



# Experimental assessment of fractal scale similarity in turbulent flows. Part 4. Effects of Reynolds and Schmidt numbers

By RICHARD D. FREDERIKSEN[1], WERNER J. A. DAHM[1] AND DAVID R. DOWLING[2]

[1] Department of Aerospace Engineering, The University of Michigan, Ann Arbor, MI 48109-2140, USA

[2] Department of Mechanical Engineering and Applied Mechanics, The University of Michigan Ann Arbor, MI 48109-2125, USA

(Received 3 September 1997 and in revised form 20 July 1998)

Experimental results are presented for the influence of Reynolds number on multifractal scale similarity in turbulent flows. These are obtained from single-point measurements of a dynamically passive $Sc \approx 1$ conserved scalar quantity $\zeta(t)$ in a turbulent shear flow at outer-scale Reynolds numbers of $14000 \leqslant Re_\delta \leqslant 110000$. Statistical criteria based on the maximum allowable scale-to-scale variation $L_1(\epsilon)$ in multiplier distributions $P(M_\epsilon)$ from multifractal gauge sets allow accurate discrimination between multifractal and non-multifractal scaling. Results show that the surrogate scalar energy dissipation rate $\chi_s(t) \equiv (\mathrm{d}\zeta/\mathrm{d}t)^2$ is found to display a scale-invariant similarity consistent with a random multiplicative cascade characterized by a bilinear multiplier distribution $P(M_\epsilon)$ over a range of scales extending downward from the outer scale $T_\delta$. For a range of scales extending upward from the inner (diffusive) scale $T_D$, the dissipation rate displays a different scale-invariant similarity characterized by a uniform multiplier distribution. The former scale-invariance becomes evident in the present $Sc \approx 1$ data only when $Re_\delta$ is sufficiently large. Comparisons with results from $Sc$ 1 data indicate that this scale-invariant similarity applies when the outer-to-inner scale ratio $T_\delta/T_D \approx 0.09\ Re_\delta^{3/4}\, Sc^{1/2}$ is greater than about 400. In contrast to the scalar dissipation rate field, the scalar field is found to lack any multifractal scale similarity.

## 1. Introduction

The wide range of length and time scales in high Reynolds number turbulent flows has led to a variety of postulates to describe the highly intermittent nature of gradient quantities such as vorticity and dissipation in these flows. Most of these invoke some type of scale similarity assumption that allows features over a range of scales to be treated within the same framework. This paper, the fourth in a series examining various aspects of scale similarity in turbulent flows, evaluates the applicability of one such postulate – the multifractal model (e.g. Hentschel & Procaccia 1983; Frish & Parisi 1985; Halsey *et al.* 1986) – to the dynamical signature produced by a turbulent shear flow in gradients of a passive scalar mixed by the flow. In particular, we present experimental results for the effects of Reynolds and Schmidt numbers on the applicability of the multifractal model, and on the range of scales over which this type of scale similarity is found.

The major conclusions from three previous parts (Frederiksen, Dahm & Dowling 1996, 1997*a*, *b*; hereinafter referred to respectively as Parts 1, 2 and 3) were concerned with the applicability of fractal and multifractal scaling concepts to conserved scalar fields $\zeta(\boldsymbol{x}, t)$ and scalar energy dissipation rate fields $\chi(\boldsymbol{x}, t) \equiv \boldsymbol{\nabla}\zeta \cdot \boldsymbol{\nabla}\zeta(\boldsymbol{x}, t)$ in turbulent flows. Those studies were based on fully resolved four-dimensional spatio-temporal laser-induced fluorescence imaging data obtained at outer-scale Reynolds number $Re_\delta$ of several thousand and Schmidt numbers $Sc$ near 2000, with the resulting $Re_\delta Sc$ product exceeding $10^7$. The measurement technique allowed examination of the scaling properties in one-, two-, or three-dimensional spatial intersections through the data volumes as well as in time. In Part 1 calibrations were introduced based on fractal and non-fractal gauge sets that allowed objective assessment of scale similarity in one-dimensional spatial and temporal intersections through the experimental data. Results showed that the support set on which $\chi(\boldsymbol{x}, t)$ is concentrated is 'as fractal as known stochastic fractal gauge sets' (fractional Brownian motion sets having the same record length). Part 2 extended these assessments to two- and three-dimensional spatial intersections with the four-dimensional data, and found that the $\chi(\boldsymbol{x}, t)$ fields remain fractal except in small inclusions within which diffusion dominates, thereby breaking the scale similarity. Part 3 examined multifractal scale similarity and introduced a rigorous assessment criterion based on the maximum allowable statistical variations in the scale-to-scale multiplier distributions $P(M_\epsilon)$. Other constructs were found to be insufficiently sensitive to robustly discriminate between multifractal and non-multifractal gauge sets. Calibrations based on known stochastic multifractal gauge sets yielded a difference norm $L_1(\epsilon)$ that could be compared to similar norms obtained from the experimental data. Results showed that $\chi$-fields reliably follow multifractal scaling between the viscous scale $\lambda_\nu$ and the diffusive scale $\lambda_D$, while the corresponding $\zeta$-fields lacked any multifractal scale similarity over this range of scales.

Prior studies on the applicability of multifractal scale similarity in turbulent flows are reviewed in Part 3. The earliest results indicating such scaling in turbulent shear flows were presented by Meneveau & Sreenivasan (1987, 1991), Prasad, Meneveau & Sreenivasan (1988), Sreenivasan & Prasad (1989) and Sreenivasan (1991*a*, *b*). Their experiments involved a variety of shear flows at Reynolds numbers ranging from typical laboratory-scale experiments to atmospheric-scale turbulence. Comparisons of the results in Parts 1–3 with these earlier studies are discussed in each of these papers. A key point is that Parts 1–3 were based on comparisons with fractal and non-fractal gauge sets, which allow direct assessments of the applicability of these scale-similarity hypotheses. Of particular relevance to the present study is the notion of scale-invariant multiplier distributions $P(M)$, introduced by Sreenivasan (1991*b*), Chhabra & Sreenivasan (1992), and Sreenivasan & Stolovitzky (1995). Note that the $P(M_\epsilon)$ distributions found in Part 3 for the scalar dissipation rate field in a comparatively low Reynolds number turbulent shear flow were strikingly similar to those found by Chhabra & Sreenivasan (1992) from velocity measurements in atmospheric turbulence (e.g. see their figure 2).

Here the investigation of multifractal scale similarity from Part 3 is extended to examine the effects of Reynolds number and, by comparison to the earlier work, Schmidt number. The assessment criteria from Part 3 are applied to fully space- and time-resolved, single-point, Rayleigh scattering measurements of a dynamically passive $Sc \approx 1$ conserved scalar field in a turbulent shear flow at outer-scale Reynolds numbers in the range $14\,000 \leqslant Re_\delta \leqslant 110\,000$. The use of single-point scalar data $\zeta(t)$ precludes construction of the true scalar energy dissipation rate $\chi(t) \equiv D\boldsymbol{\nabla}\zeta \cdot \boldsymbol{\nabla}\zeta(t)$, and for this reason we instead examine the widely-used surrogate $\chi_s(t) \sim (\mathrm{d}\zeta/\mathrm{d}t)^2$ based on

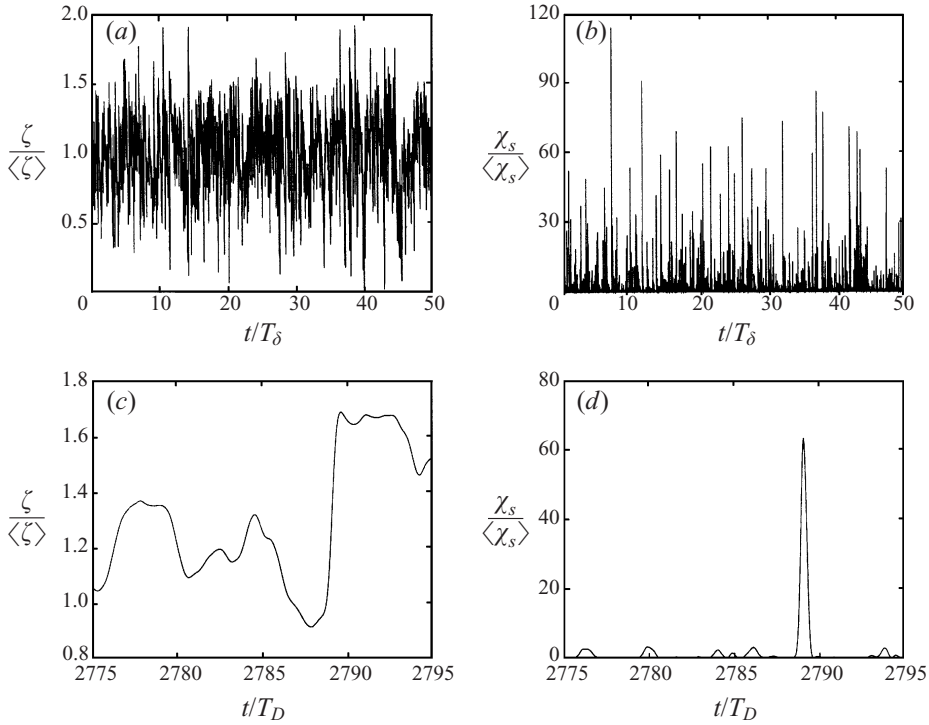


FIGURE 1. Sample traces of $\zeta(t)/\langle\zeta\rangle$ $(a, c)$ and $\chi_s(t)/\langle\chi_s\rangle$ $(b, d)$ from the present data at $Re_\delta = 14000$ shown on outer scales $(a, b)$ and on inner scales $(c, d)$.

| Case number | $Re_\delta$ | $x/d$ | $\Delta x/\lambda_D(x)$ | $\Delta t/T_D(x)$ | $\tau/T_\delta(x)$ |
|---|---|---|---|---|---|
| 56–61 | 14000 | 40 | 0.17 | 0.01 | 40 |
| 95–102 | 14000 | 60 | 0.11 | 0.01 | 60 |
| 116–118 | 44000 | 30 | 0.59 | 0.10 | 180 |
| 126–129 | 44000 | 90 | 0.49 | 0.07 | 120 |
| 132–135 | 110000 | 60 | 0.59 | 0.09 | 80 |

TABLE 1. Conditions for each of the cases considered, showing local outer-scale Reynolds number $Re_\delta$, axial location $x/d$, spatial resolution $\Delta x$ and temporal resolution $\Delta t$ relative to the local inner length and time scales $\lambda_D(x)$ and $T_D(x)$, and the measurement duration $\tau$ relative to the local outer-scale time $T_\delta(x)$. Effects of the Wiener filtering may increase $\Delta t$ by up to an order of magnitude.

Taylor's hypothesis, which retains the salient characteristics of $\chi(t)$ (Dowling 1991; Dahm & Southerland 1997). The corresponding surrogate $\Phi_s \sim (\mathrm{d}u/\mathrm{d}t)^2$ has been used in previous studies (e.g. Sreenivasan 1991*a*; Meneveau & Sreenivasan 1991) of scale similarity in the true kinetic energy dissipation rate $\Phi(t) \equiv 2\nu\epsilon{:}\epsilon(t)$, where $\epsilon(\boldsymbol{x}, t)$ is the full strain rate tensor. We examine the scaling properties of $\chi_s$ at three different Reynolds numbers.

The presentation is organized as follows. In §2 we summarize the experimental data used in the present study, and in §3 we briefly review the multifractal scale-similarity criteria that were developed in Part 3 and are employed here. Following this, §4 evaluates the applicability of scale-invariant similarity in the conserved scalar data $\zeta(t)$. Section 5 examines multiplier distributions $P(M_\epsilon)$ and scale-to-scale difference norms $L_1(\epsilon)$ for the surrogate dissipation field $\chi_s(t)$, and identifies various scale ranges over

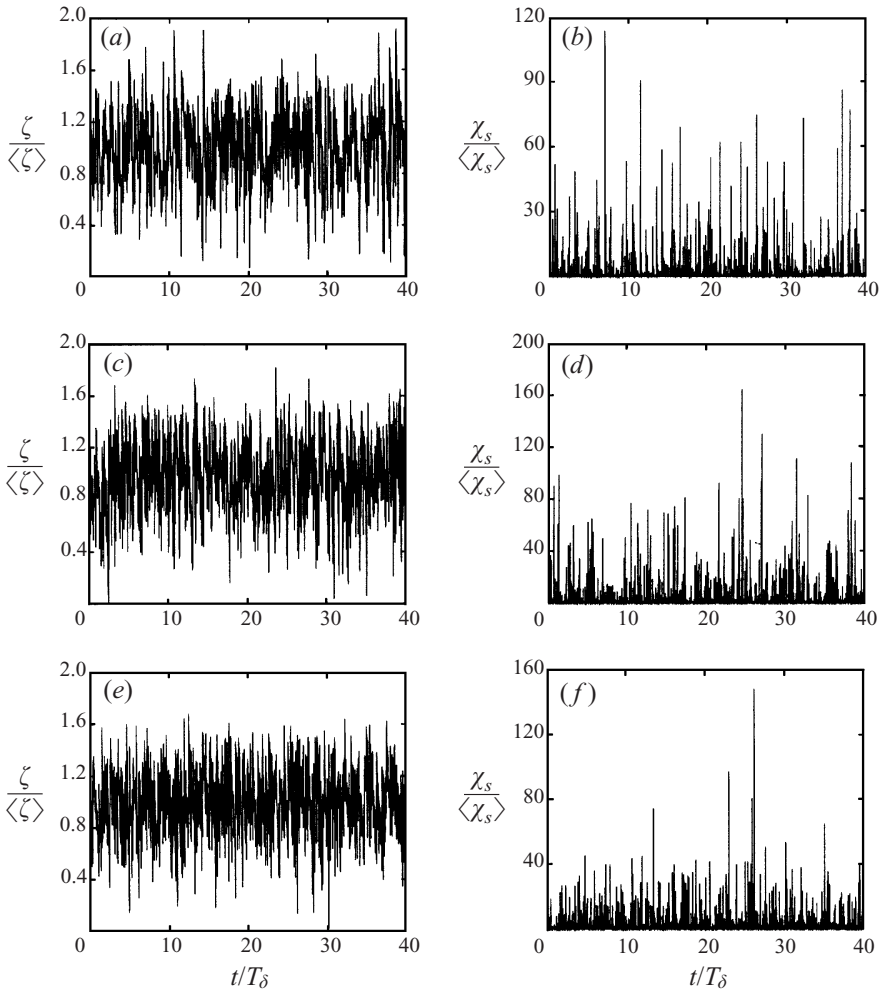


FIGURE 2. Sample traces of $\zeta(t)/\langle\zeta\rangle$ $(a, c, e)$ and $\chi_s(t)/\langle\chi_s\rangle$ $(b, d, f)$ shown on outer scales at $Re_\delta = 14000$ $(a, b)$, 44000 $(c, d)$, and 110000 $(e, f)$.

which scale-invariance applies. The effects of outer-scale Reynolds number and Schmidt number on these scaling ranges are examined in §6 by comparing with the previous measurements at $Sc$ 1. Conclusions as to the applicability of multifractal scaling concepts for characterizing the scale-similarity properties of turbulent flows are drawn in §7.

## 2. Experimental summary

The present study is based on long-record-length, single-point, fully-resolved Rayleigh scattering measurements of a conserved scalar in the self-similar far field of an axisymmetric turbulent jet of ethylene or propylene gas issuing into nitrogen or argon. Detailed descriptions of the experimental facility and measurement technique, as well as statistical validation of these data, are given by Dowling & Dimotakis (1990) and Dowling (1993).

Briefly, a jet of purified gas issues through a smoothly contoured round nozzle with exit diameter $d$ at Reynolds numbers $Re_\delta$ of 14000, 44000 and 110000 into a nominally

quiescent 1.2 m × 1.2 m × 2.3 m ambient enclosure containing a second purified gas. Here $Re_\delta \equiv (u\delta/\nu)$ is the local outer-scale Reynolds number based on the outer length scale $\delta(x) \approx 0.44x$ and centreline velocity $u(x) \approx 7.2\,(J/\rho)^{1/2}x^{-1}$ which characterize the mean shear driving the turbulence, where $J$ and $\rho$ denote the jet momentum flux and the ambient fluid density, respectively. At the lowest Reynolds number, the jet fluid was ethylene and issued at 4.0 m s$^{-1}$ through a 19.0 mm diameter nozzle into nitrogen, giving a density ratio of 1.0015 and molecular Schmidt number $Sc \equiv (\nu/D)$ of 1.0. At the two higher Reynolds numbers, the jet consisted of propylene issuing at 28.6 and 71.5 m s$^{-1}$, respectively, through a 7.62 mm diameter nozzle into argon, giving a density ratio of 1.05 and $Sc \approx 1.2$. In all cases, the jet exit turbulence level was less than 0.2 %. A weak coflow prevented recirculation within the enclosure while still providing jet-momentum-dominated flow, as verified by the outer-variable similarity scaling reported in Dowling & Dimotakis (1990).

High-resolution, single-point Rayleigh scattering measurements of jet fluid concentration were made at up to 90 jet-exit diameters (see table 1) downstream from the nozzle. The size $\Delta x$ of the focal volume from which Rayleigh scattered light was collected was adjusted (see table 1) for each $x$ and $Re_\delta$ to remain constant relative to the local scalar diffusion lengthscale $\lambda_D(x) \approx 11.2\ \delta(x)\,Sc^{-1/2}\,Re_\delta^{-3.4}$ (Southerland & Dahm 1996; Dahm, Su & Tacina 1996; Buch & Dahm 1996, 1998) except at the lowest $Re_\delta$, where the spatial resolution is roughly four times higher. Likewise the sampling interval $\Delta t$ for each measurement, typically consisting of a record length of $2^{19}$ samples spanning a duration $\tau$ of 60 to 180 local outer timescales $T_\delta(x) \equiv \delta(x)/u(x)$, was also adjusted (see table 1) to remain constant relative to the local inner lengthscale advection time $T_D(x) \equiv \lambda_D(x)/u(x)$ except at the lowest $Re_\delta$. Spectral and statistical quantities derived from these data (Dowling & Dimotakis 1990) verify that the measurements were spatially and temporally resolved, as well as statistically converged.

To allow accurate differentiation in the present study, the measured jet fluid concentrations $\zeta(t)$ were Wiener filtered (e.g. Press *et al.* 1986) and $\chi_s(t)$ was computed via central differencing of the filtered data. Figures 1 and 2 show representative time traces of $\zeta(t)/\langle\zeta\rangle$ and $\chi_s(t)/\langle\chi_s\rangle$, where $\langle\cdot\rangle$ denotes the time average of the corresponding trace. The data in figure 1 are for the lowest $Re_\delta$, and illustrate the dynamic range and temporal resolution of the measurements.

## 3. Multifractal scale-similarity criterion

A rigorous assessment criterion capable of reliably discriminating between multifractal and non-multifractal sets was developed in Part 3 and is adopted here. The method is based on the maximum allowable statistical variation at scale $\epsilon$ in the distribution $P(M_\epsilon)$ of multipliers $M_\epsilon$ obtained from analyses of a set of measures $\mu(t)$ derived from the original sets $\zeta(t)/\langle\zeta\rangle$ or $\chi_s(t)/\langle\chi_s\rangle$. Criteria based on other classical multifractal constructs, such as partition functions $X_q$ or dimensions $f(\alpha)$, were clearly shown in Part 3 to be insufficiently sensitive to discriminate non-multifractal from multifractal gauge sets. For this reason, results for such constructs are not presented here. Instead, objective assessment of multifractal scaling is obtained by comparing the $L_1(\epsilon)$ difference norm between successive $P(M_\epsilon)$ with the corresponding curve derived from a known stochastic multifractal gauge set. A data set can thereby be rigorously declared either to be or not to be 'as multifractal as the multifractal gauge set'.

The measures $\mu(t_i)$ at each scale $\epsilon$ are simply the average value of the original data set $\zeta(t)/\langle\zeta\rangle$ or $\chi_s(t)/\langle\chi_s\rangle$, multiplied by the relative interval size $\epsilon/L$, within contiguous time intervals of scale $\epsilon$ centred at times $t_i$ covering the entire record length

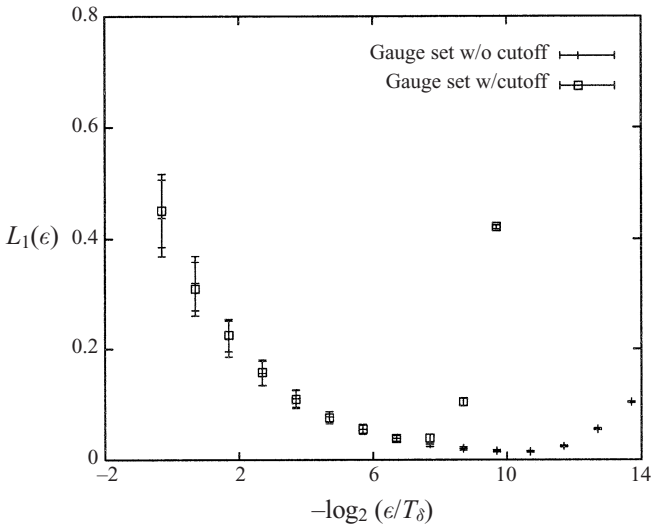


FIGURE 3. Scale-to-scale variations $L_1(\epsilon)$ in multiplier distributions $P(M_\epsilon)$ for a pure stochastic multifractal gauge set and a multifractal gauge set with an inner cut-off.

$L$ (see (6) of Part 3). In practice, the $\epsilon$ are incremented in factors of 2, with the largest $\epsilon$ corresponding to $L$ and the smallest containing just two data points. For records consisting of $2^n$ equally spaced points, scale similarity can be examined at $n-1$ different scales. From the resulting set of measures $\mu(t_i)$ at each scale $\epsilon$, a set of multipliers $M_\epsilon(t_i)$ is constructed via (8) of Part 3, which are simply the ratio of the measures at successive scales for each point in the set, and are thus bounded by $0 \leqslant M_\epsilon \leqslant 1$.

The multipliers $M_\epsilon$ at each scale $\epsilon$ produce the multiplier distribution $P(M_\epsilon)$, which will show statistical variations if the record length is finite. If there are many data sets at identical conditions, as in Part 3, then their individual multiplier distributions can be ensemble averaged to give $\langle P(M_\epsilon)\rangle$ with higher statistical convergence. A further increase in statistical convergence is obtained by effectively generating the average multiplier distribution in both directions of time by symmetrizing $P(M_\epsilon)$.

If the resulting distributions $P(M_\epsilon)$ are scale-invariant over a range of $\epsilon$, then the data set displays multifractal scale similarity. The assessment of scale-invariance is based on the $L_1$ difference norm

$$L_1(\epsilon) \equiv \int_M |P(M_\epsilon) - P(M_{\epsilon/2})|\,\mathrm{d}M \tag{1}$$

characterizing the scale-to-scale variation in $P(M_\epsilon)$. The maximum allowable statistical variation between any two successive scales is set by the corresponding results for a known stochastic multifractal gauge set. Based on the findings in Part 3, a scale-similar random multiplicative cascade with bilinear $P(M)$ is used to generate $L_1(\epsilon)$ in figure 3, against which all results obtained here will be compared. The error bars shown are the result of 10000 individual realizations of this multifractal gauge set. The figure shows the results obtained when this scale similarity is taken to apply over the entire range of scales. Also shown is the effect of a diffusive cutoff scale, below which $P(M) \equiv 0.5$ is used to generate the gauge sets.

For later reference, note that if $P(M_\epsilon)$ is strongly peaked near $M = \frac{1}{2}$, then the measures in adjacent intervals at that scale are nearly equal. This will occur for very

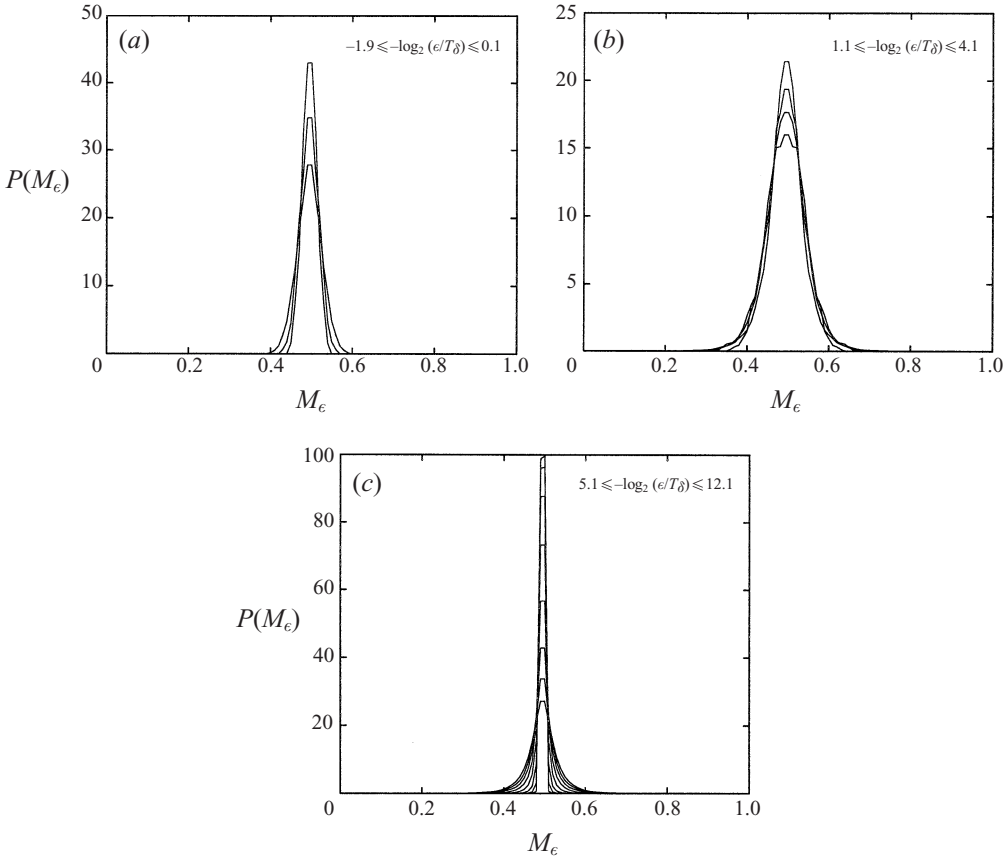


FIGURE 4. Multiplier distributions $P(M_\epsilon)$ obtained from the scalar field data $\zeta(t)/\langle\zeta\rangle$ at $Re_\delta = 44000$. Note the lack of any scale-invariant distribution.

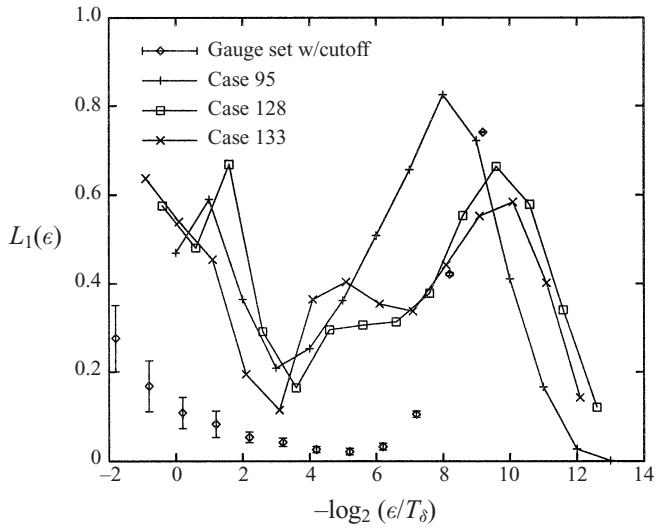


FIGURE 5. Comparison of scale-to-scale variations $L_1(\epsilon)$ in multiplier distributions $P(M_\epsilon)$ from scalar field data at $Re_\delta = 44000$ with multifractal gauge sets.

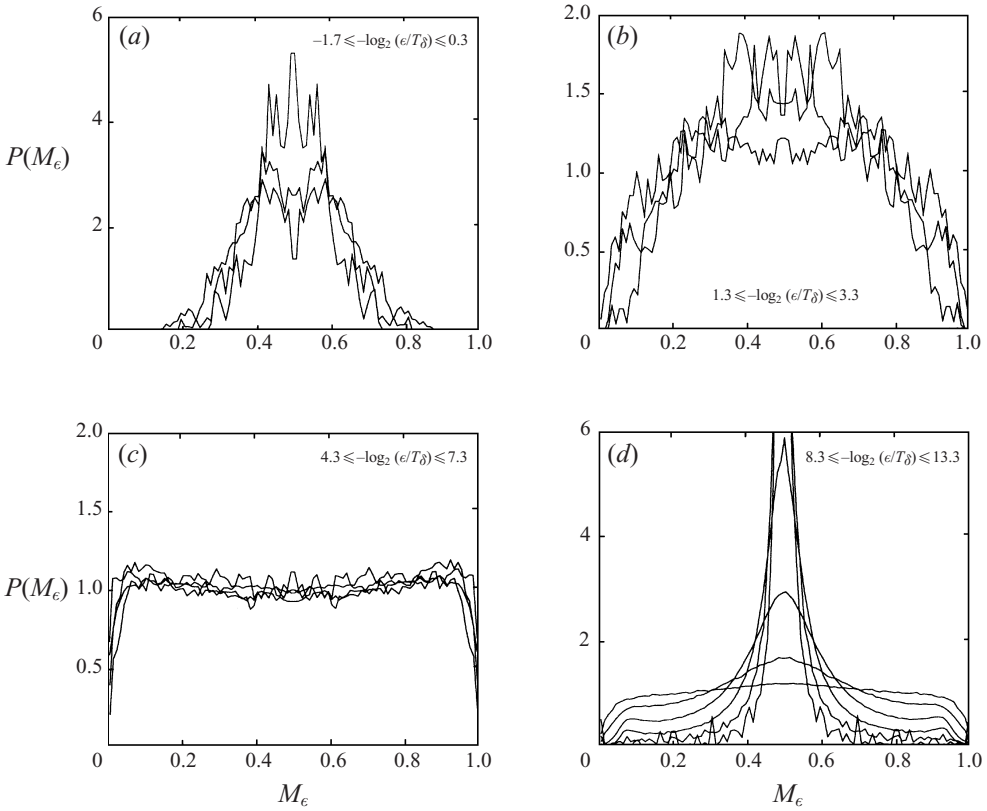


FIGURE 6. Multiplier distributions $P(M_\epsilon)$ obtained from dissipation rate data $\chi_s(t)/\langle\chi_s\rangle$ at $Re_\delta = 44000$.

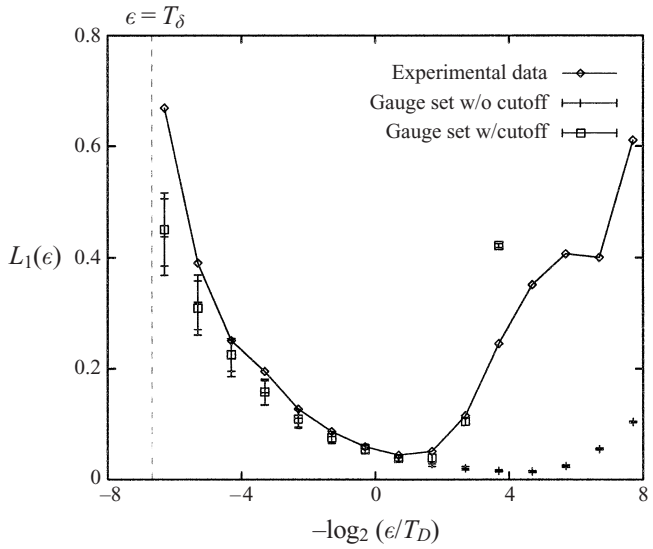


FIGURE 7. Comparison of scale-to-scale variation $L_1(\epsilon)$ is multiplier distributions $P(M_\epsilon)$ from figure 6 at $Re_\delta = 44000$ with multifractal gauge sets.

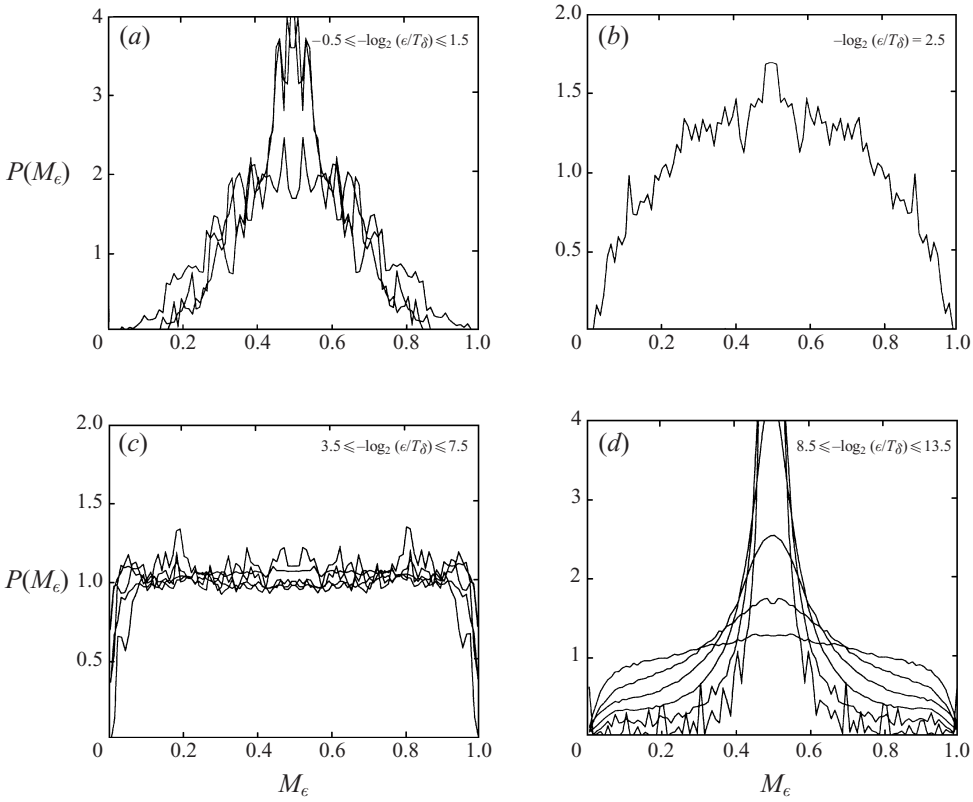


FIGURE 8. Multiplier distributions $P(M_\epsilon)$ obtained from dissipation rate data $\chi_s(t)/\langle\chi_s\rangle$ at $Re_\delta = 14000$.

large scales, at which the measure in any interval must approach the average value of the set being examined, as well as at exceedingly small scales, on which the set shows essentially no structure and thus the measures in adjacent intervals will again be nearly equal. On the other hand, if $P(M_\epsilon)$ is nearly uniform then all possible multipliers are equally likely, indicating that there is no correlation between the measures $\mu(t_i)$ in adjacent intervals at that scale.

## 4. $\zeta(t)$ versus $\chi_s(t)$ scalings

The applicability of multifractal scale similarity to the conserved scalar field data $\zeta(t)$ will be examined first. Note that there are reasons to question such a hypothesis on fundamental grounds; however, multifractal scale similarity in the scalar field has been postulated by Chechetkin, Lutovinov & Turygin (1990) and Shivamoggi (1992), as noted in Part 3. Figure 4 shows the multiplier distributions $P(M_\epsilon)$ obtained from the conserved scalar set $\zeta(t)$ for Case 128 in table 1. The results are typical of those obtained for $\zeta(t)$ at all values of $Re_\delta$. No scale similarity whatsoever is seen in the results, as is evident by the lack of any collapse of the $P(M_\epsilon)$ onto a scale-independent distribution. This can be readily seen in figure 5, where the resulting scale-to-scale difference norm $L_1(\epsilon)$ is compared with the corresponding result from known multifractal gauge sets as discussed above. Also shown are the results obtained from a number of other cases in table 1. In all cases, the $L_1(\epsilon)$ are far too high to meet the requirements for scale similarity.

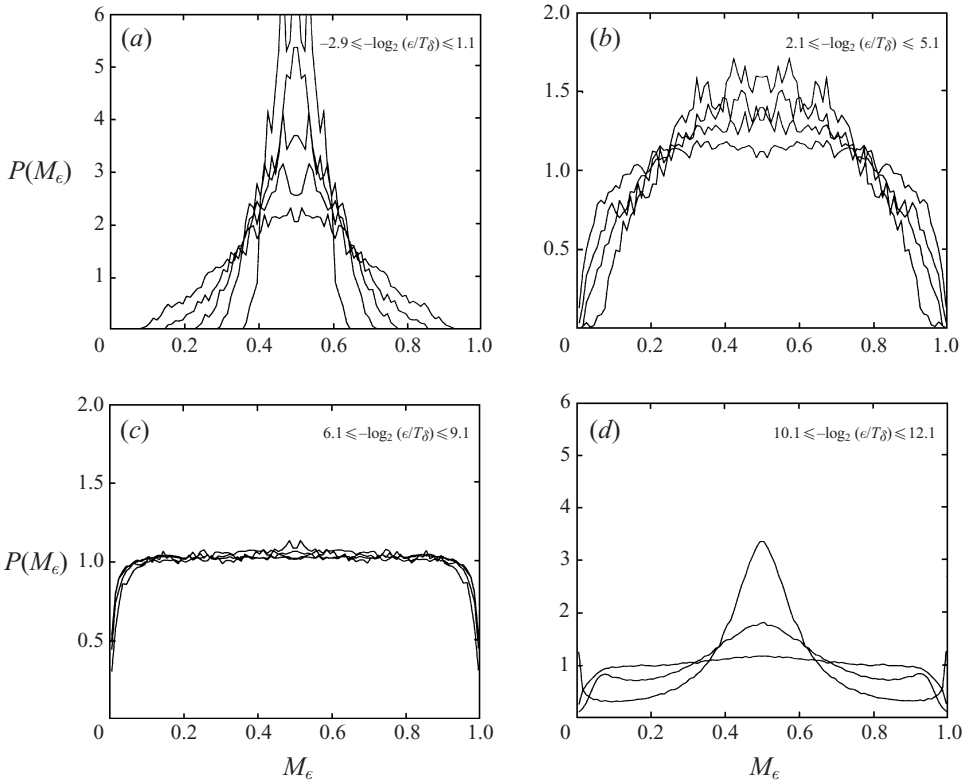


FIGURE 9. Multiplier distributions $P(M_\epsilon)$ obtained from dissipation rate data $\chi_s(t)/\langle\chi_s\rangle$ at $Re_\delta = 44000$.

Figure 6 shows the multiplier distributions $P(M_\epsilon)$ obtained from the surrogate scalar dissipation rate field $\chi_s(t)$ for the case examined in figure 4. Unlike the scalar field results, the dissipation field shows indications of possible scale-invariance over several ranges of scales. To test this we examine the corresponding $L_1(\epsilon)$ shown in figure 7, where it can be seen that, over certain scale ranges, the results are much closer to those obtained from multifractal gauge sets. This will be examined in more detail in §5; however, at this point we can already conclude that the measured conserved scalar sets $\zeta(t)$ clearly do not show any scale similarity of the type examined here, at any Reynolds number or axial location in the flow. Dissipation sets $\chi_s(t)$ from precisely the same data, on the other hand, do show possible multifractal scale similarity, and for this reason the remainder of this study will deal only with these fields.

## 5. Scale-similarity ranges in $P(M_\epsilon)$ and $L_1(\epsilon)$

### 5.1. *Multiplier distributions $P(M_\epsilon)$*

Figure 8 shows the multiplier distributions $P(M_\epsilon)$ obtained for Case 95 in table 1, corresponding to the measurement at the lowest $Re_\delta$ (highest resolution), for scales $\epsilon$ from $-0.5 \leqslant -\log_2(\epsilon/T_\delta) \leqslant 13.5$. The distributions are shown in separate groups covering various scale ranges. Multiplier distributions obtained at $Re_\delta = 44000$ and 110000 are shown in figures 9 and 10. Note that the range of scales shown in each panel is normalized with outer variables. The results in figure 9 should be compared with those in figure 6, which were obtained at the same $Re_\delta$. Note that these two sets

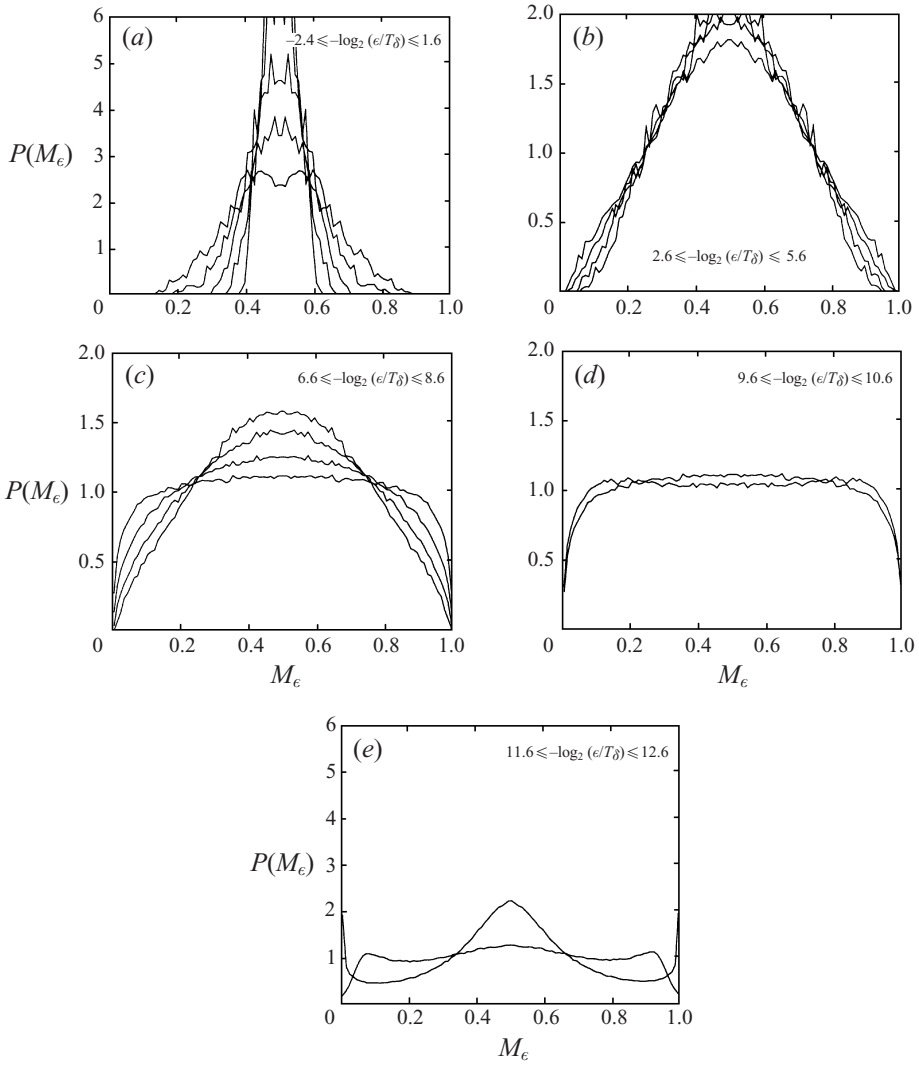


FIGURE 10. Multiplier distributions $P(M_\epsilon)$ obtained from dissipation rate data $\chi_s(t)/\langle\chi_s\rangle$ at $Re_\delta = 110000$.

of multiplier distributions are very nearly identical, indicating that $P(M_\epsilon)$'s obtained from a single data set in these measurements appear to be representative of the true scaling properties of the flow at that $Re_\delta$.

There are several distinguishing features of these distributions that become apparent in such comparisons. Note that panel (*a*) in each figure, corresponding to the scaling at very large scales, shows $P(M_\epsilon)$ increasingly accumulating at $M = \frac{1}{2}$ as the scale size $\epsilon$ increases. Similarly panel (*d*) in each figure, giving the scaling at very small scales, shows $P(M_\epsilon)$ accumulating at $M = \frac{1}{2}$ as the scale size $\epsilon$ decreases. This is expected from the discussion at the end of §3, since in both these scale limits the measures in adjacent intervals must become asymptotically equal. These regimes will be denoted I and V.

Putting these trivial scaling regimes aside, we next examine the apparently uniform $P(M_\epsilon)$ seen at $Re_\delta = 14000$ in figure 8(*c*), and in figure 9(*c*) at $Re_\delta = 44000$ and figure 10(*d*) at $Re_\delta = 110000$. This regime will be denoted IV. Objective assessment of

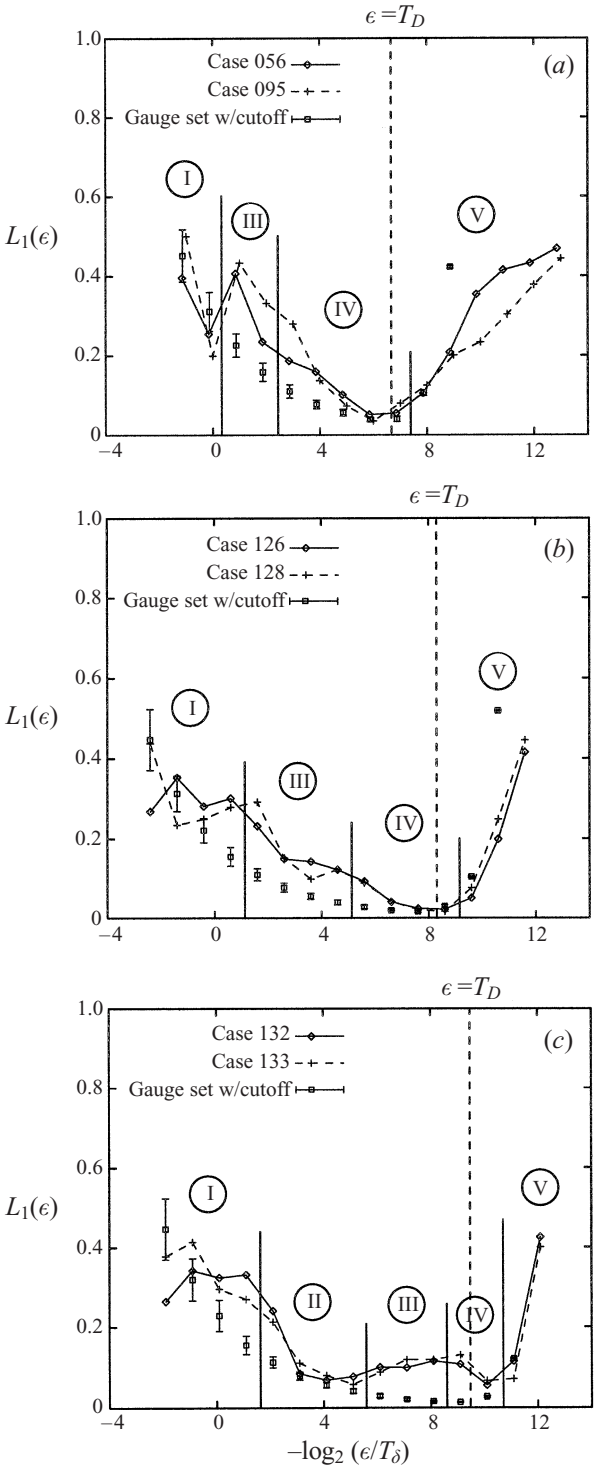


FIGURE 11. Comparison of scale-to-scale variation $L_1(\epsilon)$ in multiplier distributions $P(M_\epsilon)$ from figures 8–10 with multifractal gauge sets, showing results obtained at $Re_\delta = 14000$ (*a*), 44000 (*b*), and 110000 (*c*).

possible scale similarity in this range of scales from the difference norms $L_1(\epsilon)$ will be given below. For now we note that the presence of such a uniform multiplier distribution indicates that, over this range of scales, the measures obtained from adjacent intervals in the dissipation field are essentially uncorrelated, as was noted in §3. This result in terms of the multiplier distributions $P(M_\epsilon)$ is, in effect, equivalent to the observation by Sreenivasan & Prasad (1989) that the generalized dimensions $D_q$ (see Part 3) over this range of scales are essentially independent of the order of the moment. Note that this regime is seen to extend over a range of $2^4$ to $2^5$ in the scales at the two lower $Re_\delta$. At the highest $Re_\delta$, the narrower range of scales may be due to the Wiener filtering applied.

A second regime showing possible scale similarity is found at larger scales for $Re_\delta = 110000$, as seen in figure 10(*b*), and will be denoted regime II. Objective examination of this apparent similarity will also be given below, but here we observe that the shape of the multiplier distributions $P(M_\epsilon)$ over this range of scales is very different from that found above. Note in particular that $P(M_\epsilon)$ is roughly bilinear, and that this form is only seen at the highest $Re_\delta$. A bilinear multiplier distribution was also found by Chhabra & Sreenivasan (1992) at much higher Reynolds numbers in analyses of the surrogate kinetic energy dissipation rate field from velocity measurements in atmospheric turbulence.

Recall also from Part 3 that a bilinear multiplier distribution similar to that seen in figure 10(*b*) was found in that study at comparable scales for $Re_\delta = 5200$ but with $Sc = 2075$, giving the Peclét number $Re_\delta Sc \approx 10^7$. In the present case $Re_\delta Sc = 10^5$, suggesting the possibility that this shape may be a characteristic of high-Peclét-number conserved scalar mixing. Here this similarity appears to extend over a range of $2^4$ in scales, whereas in Part 3 it was found over a range of $2^7$ in scales, again consistent with some type of Peclét number scaling. The bilinear shape of $P(M_\epsilon)$ at these scales indicates a significant correlation among measures derived from the dissipation in adjacent intervals, which appears to be a characteristic of high-Reynolds-number (possibly high-Peclét-number) scalar dissipation rate fields. The possibility of a Peclét number scaling is examined in §6.

The only remaining scales are between II and IV, and can be seen in figures 8(*b*), 9(*b*), and 10(*c*). This range will be denoted III. Over these scales, the multiplier distributions $P(M_\epsilon)$ undergo a transition from the bilinear form that appears in II at sufficiently high $Re_\delta$ and $Sc$ to the uniform distribution found in IV at all $Re_\delta$. In figure 10(*c*) this transition regime spans a range of $2^3$ in scales.

### 5.2. *Scale-to-scale difference norms* $L_1(\epsilon)$

Figure 11 shows the $L_1(\epsilon)$ difference norms between the multiplier distributions $P(M_\epsilon)$ obtained at $Re_\delta = 14000$, 44000 and 110000. Also shown are the results from gauge sets based on a random multiplicative cascade having the bilinear multiplier distribution noted above, and the small-scale cutoff described in §3. The five scale ranges identified in §5.1 are shown in each panel, with the boundaries obtained by inspection of the $P(M_\epsilon)$ distributions in figures 6, 8, 9 and 10. Figure 12 schematically indicates the scaling phenomena that lead to the five scale ranges identified above.

The scale $\epsilon/T_\delta \approx \frac{1}{4}$ at which Region I ends can be seen in figure 11(*a–c*) to be nearly independent of $Re_\delta$, as might be expected if this is set by the outer (inviscid) scales of the flow. It seems reasonable that the scaling of measures on intervals larger than this will be dominated by the required approach to the average value, as indicated in figure 12, with the attendant trivial limit $M \to \frac{1}{2}$ in $P(M_\epsilon)$, and that on intervals smaller than this the scaling of measures will be dominated by the structure of $\chi_s(t)$.

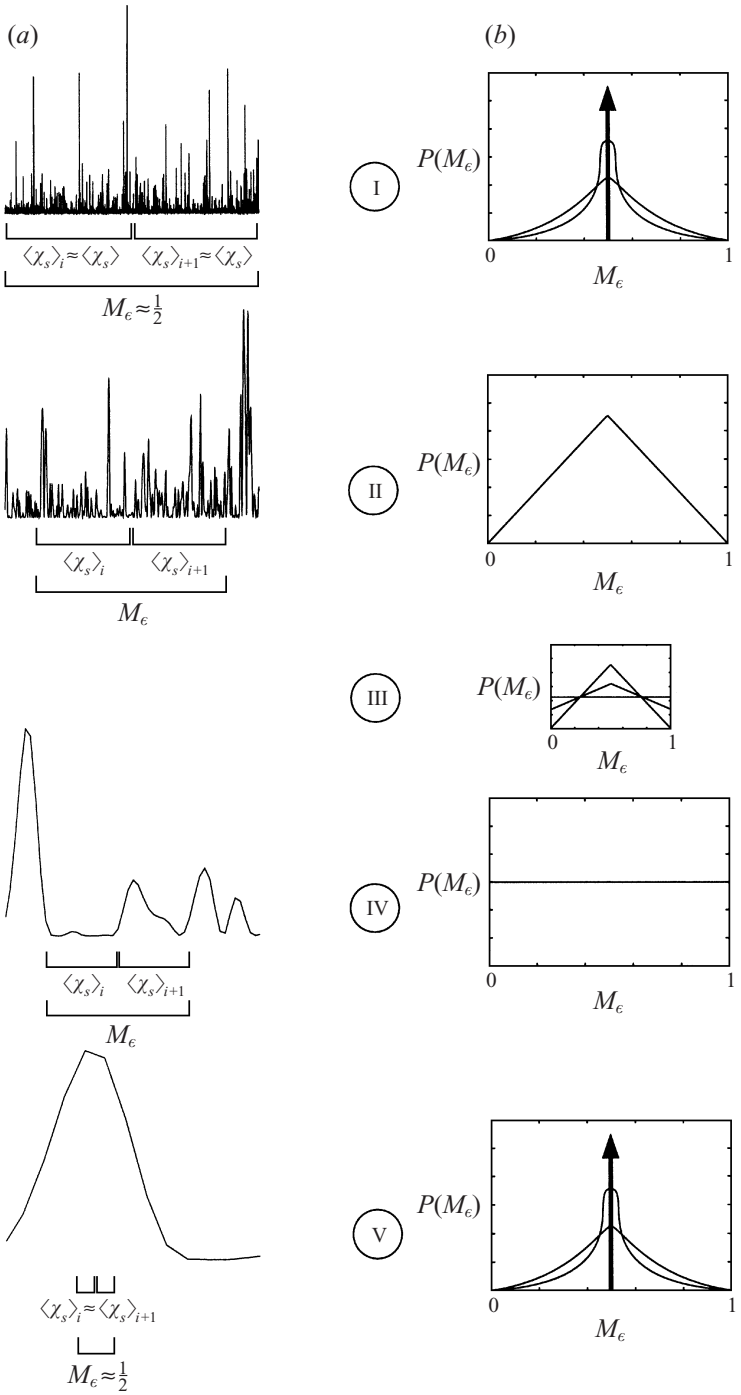


FIGURE 12. Schematic showing dissipation sets on various scales (*a*) and multiplier distributions in each scaling range (*b*).

At the other extreme, the scale at which Region V begins can be seen in figure 11(*a–c*) to be set by the inner (diffusive) scales of the flow. This limit lies near $\epsilon/T_D \approx \frac{1}{4}$, and is otherwise independent of $Re_\delta$. This limiting value also appears reasonable since, as indicated in figure 12, the scaling on intervals smaller than this will be dominated by the required approach of measures on adjacent intervals to the same value, again with the resulting trivial limit $M \to \frac{1}{2}$ in $P(M_\epsilon)$. Consistent with the resolution evident in figure 1(*d*), Region V thus reflects scales much smaller than the dissipation layer thickness at which no scale similarity is present.

Region IV should then reflect scales comparable to the dissipation layer thickness, and indeed in all cases in figure 11(*a–c*) the diffusion-scale advection time $\epsilon/T_D \approx 1$ lies within the observed Region IV. Measures on adjacent intervals in this range of scales will be largely uncorrelated, leading to the uniform $P(M_\epsilon)$. In many instances only one of these intervals may contain most of the dissipation, as indicated in figure 12. Related to this, it must be noted that the similarity found over this range of scales may be an artifact of $\chi_s(t)$ that will not be present in the true dissipation field $\chi(t)$. The surrogate dissipation contains a wider range of apparent 'thicknesses' $T_D$ produced as dissipation layers with a relatively narrow range of true thicknesses $\lambda_D$ advect at various orientations and speeds through the measurement volume. Indeed, no scale-similarity regime with a uniform $P(M_\epsilon)$ was found for the true dissipation field $\chi(t)$ in Part 3. Finally, the range of scales over which Region IV extends might then be expected to be insensitive to $Re_\delta$, and this is largely the case in figure 11, though the range appears somewhat narrower at the highest Reynolds number. This may simply be an artifact of the Wiener filtering at this Reynolds number.

## 6. Effects of $Re_\delta$ and $Sc$

Regions II and III represent the range of scales that are of primary interest, since they reflect the signature of the small- and fine-scale structure of the underlying turbulent flow on the scalar mixing process. Region II in particular is of interest, since the $P(M_\epsilon)$ in figure 10 indicate a possible multifractal scale similarity with a simple bilinear multiplier distribution, reminiscent of the results found in Part 3 and in Chhabra & Sreenivasan (1992). Both these regions must lie between Region I, the lower end of which scales with outer variables $u$ and $\delta$, and Region IV, the upper end of which apparently scales with inner (diffusive) variables $\lambda_D$ and $D$, the scalar diffusivity. As a consequence, the extent of Regions II and III will depend on the outer-to-inner scale ratio

$$\frac{T_\delta}{T_D} \approx \frac{1}{11.2} Re_\delta^{3/4} Sc^{1/2}. \tag{2}$$

For the present $Sc \approx 1$ data, the results in figure 11 indicate that, at the lowest value of $Re_\delta$ (figure 11*a*), the scale ratio $T_\delta/T_D$ is so small that Region II is not even present and Region III is relatively narrow. At the intermediate $Re_\delta$ (figure 11*b*), for which $T_\delta/T_D \approx 250$, Region II is still not present but Region III is now much wider. It is only at the highest $Re_\delta$ (figure 11*c*) that the outer-to-inner scale ratio $T_\delta/T_D \approx 500$ in these data is large enough to accommodate a Region II spanning a significant range of scales, while the previous Region III appears simply to have been shifted to smaller scales.

The resulting Region II displays multifractal scale similarity with a bilinear $P(M_\epsilon)$, as was also found in Part 3. Relevant to this, note that for the results in Part 3, where $Sc \approx 2000$, the resulting outer-to-inner scale ratio was $T_\delta/T_D \approx 1000$ even though in that case $Re_\delta$ was only about 4000. Similarly, for the atmospheric data of Chhabra & Sreenivasan (1992), which also found a bilinear multiplier distribution, this scale ratio

is also expected to be very large. Based on that and the results obtained here, we conclude that multifractal scale similarity with a bilinear $P(M_\epsilon)$ over the range of scales in Region II appears to be the natural equilibrium scaling relevant to scalar dissipation rate fields in turbulent flows whenever the scale ratio $T_\delta/T_D$ is sufficiently large, namely whenever $Re_\delta$ and $Sc$ together satisfy the requirement that $0.09 Re_\delta^{3/4} Sc^{1/2}$ is greater than about 400. This can be achieved at surprisingly low $Re_\delta$ if $Sc$ is very large, as in Part 3.

These scale ranges and their variation with $Re_\delta$ are summarized in figure 13. At all three values of $Re_\delta$ indicated, the extent of I is the same, since this regime is set by outer-scale processes, which are inherently inviscid and thus unaffected by Reynolds number changes. In the same way, IV and V are set entirely by the diffusive processes occurring at the inner scale, and consequently the widths of these scaling ranges are independent of $Re_\delta$ and their location is set by $Re_\delta^{3/4} Sc^{1/2}$. The width of III is presumed to be independent of $Re_\delta$ and $Sc$ since it results simply from the transition between II and IV. The width of II is set by $Re_\delta^{3/4} Sc^{1/2}$.

## 7. Conclusions

This study has examined the (surrogate) scalar energy dissipation rate field $\chi_s(t)$ for stochastic multiplicative scale similarity at temporal scales ranging from more than an order of magnitude larger than the local outer timescale $T_\delta$ down to tenths or hundredths of the local inner (diffusive) advection timescale $T_D$. Existing high-resolution single-point temporal data were interrogated with an objective assessment criterion developed in Part 3, based on scale-to-scale difference norms $L_1(\epsilon)$ between multiplier distributions $P(M_\epsilon)$ at successive scales, to determine whether or not each set displays scale similarity that is 'as multifractal as a stochastic multifractal gauge set having the same record length and similar multiplier distribution'.

The present results, obtained at $Sc \approx 1$, combined with those obtained at $Sc \gg 1$ in Part 3, indicate that the scalar energy dissipation rate field $\chi(\boldsymbol{x}, t)$ in turbulent shear flows displays a scale-invariant similarity consistent with multifractal theory. In the present data, scale similarity was found over two ranges of scales, here identified as Regions II and IV. Region II is non-trivial, and occurs at scales traditionally associated with a turbulent scale-similar 'cascade'. This region, characterized by a bilinear multiplier distribution, exists at $Sc \approx 1$ only when the outer-scale Reynolds number $Re_\delta$ is large enough to accommodate a sufficiently large outer-to-inner scale ratio $T_\delta/T_D$. However for $Sc \gg 1$ this condition can be met at surprisingly low values of $Re_\delta$, even though the resulting outer-to-viscous scale ratio $T_\delta/T_\nu$ is presumably not large enough to accommodate a scale-invariant range in the underlying velocity field. The bilinear multiplier distributions found in this range are strikingly similar to those obtained by Chhabra & Sreenivasan (1992) from velocity measurements at much higher Reynolds numbers in atmospheric turbulence, suggesting that this form is a fundamental characteristic of all turbulent flows having a sufficiently wide outer-to-inner scale ratio.

The scaling found here in Region IV is characterized by a uniform multiplier distribution $P(M_\epsilon)$ and was always present, independent of $Re_\delta$. This scaling appears to be a consequence of the inner-scale structure of the flow, where over a range of temporal scales somewhat larger than the local inner-lengthscale advection time $T_D$ (and presumably a range of spatial scales near $\lambda_D$), there is essentially no correlation between the measures in adjacent intervals. The fact that no Region IV scaling has previously been found may be due in part to the higher resolution, relative to $T_D$, of the present $Sc \approx 1$ data than of the $Sc \gg 1$ data in Part 3.

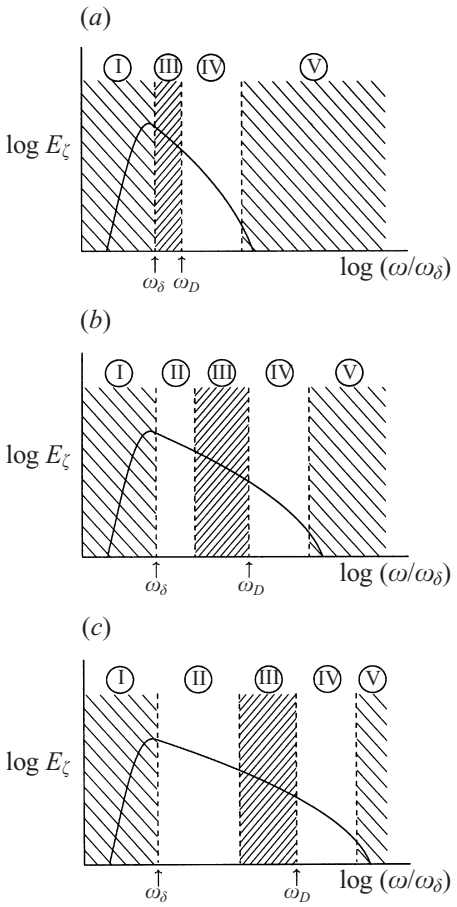


FIGURE 13. Schematic representation of $Re_\delta$ and $Sc$ effects on scaling ranges discussed in §6.

Additionally, it must be kept in mind that the results in Part 3 were obtained for the true scalar dissipation rate field $\chi(t)$, while those reported here are for the widely used surrogate dissipation $\chi_s(t)$. The apparent differences between $\chi_s(t)$ and the true scalar dissipation rate (see Dahm & Southerland 1997) occur primarily at the smallest scales. As a consequence, the Region IV scale similarity noted above may be influenced by these differences. However, at the larger scales in Region II, the differences between $\chi_s(t)$ and $\chi(t)$ should be small. The present results thus strongly indicate that $\chi(\boldsymbol{x}, t)$ displays multifractal scale similarity over this range of scales. Indeed, for the kinetic energy dissipation, numerical studies (e.g. Wang *et al.* 1996; §5) have indicated largely similar scaling of the true dissipation and its surrogate based on $(\mathrm{d}u/\mathrm{d}t)^2$ as noted in §1, though there are subtle differences.

The present $Sc \approx 1$ scalar fields were clearly found to lack any multifractal scale similarity over any range of scales, consistent with the conclusion reached in Part 3 for $Sc$ 1 scalar fields. The applicability of fractal scale similarity to isoscalar surfaces, and to scalar level crossing sets, was addressed in Part 1 for $Sc$ 1 scalar fields. The level crossing sets were found there to be clearly non-fractal, and the Schmidt number is unlikely to alter this conclusion.

This work was supported by the Air Force Office of Scientific Research (AFOSR)

under AFOSR Grant No. F49620-95-1-0115 and with discretionary funds from The University of Michigan. The measurements were made by D. R. D. at GALCIT during 1987–88 under separate support from the Gas Research Institute (GRI) and AFOSR.

## REFERENCES

Buch, K. A. & Dahm, W. J. A. 1996 Experimental study of the fine-scale structure of conserved scalar mixing in turbulent shear flows. Part 1. $Sc \quad 1$. *J. Fluid Mech.* **317**, 21–71.

Buch, K. A. & Dahm, W. J. A. 1998 Experimental study of the fine-scale structure of conserved scalar mixing in turbulent shear flows. Part 2. $Sc \approx 1$. *J. Fluid Mech.* **364**, 1–29.

Chechetkin, V. R., Lutovinov, V. S. & Turygin, A. Y. 1990 Multifractal structure of fully developed hydrodynamic turbulence. II. Intermittency effects in the distribution of passive scalar impurities. *J. Statist. Phys.* **61**, 589–605.

Chhabra, A. B. & Sreenivasan, K. R. 1992 Scale invariant multiplier distributions in turbulence. *Phys. Rev. Lett.* **68**, 2762–2765.

Dahm, W. J. A. & Southerland, K. B. 1997 Experimental assessment of Taylor's hypothesis and its applicability to dissipation estimates in turbulent flows. *Phys. Fluids* **9**, 2101–2107.

Dahm, W. J. A., Su, L. K. & Tacina, K. M. 1996 Four-dimensional measurements of vector fields in turbulent flows. *AIAA Paper* 96-1987.

Dowling, D. R. 1991 The estimated scalar dissipation rate in gas-phase turbulent jets. *Phys. Fluids* A **3**, 2229–2246.

Dowling, D. R. 1993 Mixing in gas-phase turbulent jets. In *Encyclopedia of Fluid Mechanics*, *Supplement 2: Advances in Multiphase Flow*, (ed. N. Cheremisinoff), pp. 1–25. Gulf.

Dowling, D. R. & Dimotakis, P. E. 1990 Similarity of the concentration field of gas-phase turbulent jets. *J. Fluid Mech.* **218**, 109–141.

Frederiksen, R. D., Dahm, W. J. A. & Dowling, D. R. 1996 Experimental assessment of fractal scale similarity in turbulent flows. Part 1. One-dimensional intersections. *J. Fluid Mech.* **327**, 35–72.

Frederiksen, R. D., Dahm, W. J. A. & Dowling, D. R. 1997*a* Experimental assessment of fractal scale similarity in turbulent flows. Part 2. Higher dimensional intersections and non-fractal inclusions. *J. Fluid Mech.* **338**, 89–126.

Frederiksen, R. D., Dahm, W. J. A. & Dowling, D. R. 1997*b* Experimental assessment of fractal scale similarity in turbulent flows. Part 3. Multifractal scaling. *J. Fluid Mech.* **338**, 127–155.

Frisch, U. & Parisi, G. 1985 In *Turbulence and Predictability in Geophysical Fluid Mechanics and Climate Dynamics* (ed. M. Ghil, R. Benzi & G. Parisi). North-Holland.

Halsey, T. C., Jensen, N. H., Kadanoff, L. P., Procaccia, I. & Shraiman, B. I. 1986 Fractal measures and their singularities: The characterization of strange sets. *Phys. Rev.* A **33**, 1141–1151.

Hentschel, H. G. E. & Procaccia, I. 1983 The infinite number of generalized dimensions of fractals and strange attractors. *Physica* D **8**, 435–444.

Meneveau, C. & Sreenivasan, K. R. 1987 Simple multifractal cascade model for fully developed turbulence. *Phys. Rev. Lett* **59**, 1424–1427.

Meneveau, C. & Sreenivasan, K. R. 1991 The multifractal nature of the turbulent energy dissipation. *J. Fluid. Mech.* **224**, 429–484.

Prasad, R. R., Meneveau, C. & Sreenivasan, K. R. 1988 The multifractal nature of the dissipation field of passive scalar in fully turbulent flows. *Phys. Rev. Lett* **61**, 74–77.

Press, W. H., Flannery, B. P., Teukolsky, S. A. & Vetterling, W. T. 1986 In *Numerical Recipes*, pp. 415–420. Cambridge University Press.

Shivamoggi, B. K. 1992 Multi-fractal aspects of the intermittency corrections to the spectrum of temperature fluctuations in isotropic turbulence. *Phys. Lett.* A **168**, 47–54.

Southerland, K. B. & Dahm, W. J. A. 1996 Fully-resolved four-dimensional measurements of the small-scale structure of passive scalar mixing in turbulent flows. *Rep.* 026779-12. Dept. of Aerospace Engineering, The University of Michigan (Ann Arbor).

Sreenivasan, K. R. 1991*a* Fractals and multifractals in fluid turbulence. *Ann. Rev. Fluid Mech.* **23**, 539–600.

Sreenivasan, K. R. 1991*b* On local isotropy of passive scalars in turbulent shear flows. *Proc. R. Soc. Lond.* A **434**, 165–182.

Sreenivasan, K. R. & Prasad, R. R. 1989 New results on the fractal and multifractal structure of the large Schmidt number passive scalars in fully turbulent flows. *Physica* D **38**, 322–329.

Sreenivasan, K. R. & Stolovitzky, G. 1995 Turbulent cascades. *J. Statist. Phys.* **78**, 311–333.

Wang, L.-P., Chen, S., Brasseur, J. G. & Wyngaard, J. C. 1996 Examination of hypotheses in the Kolgomorov refined turbulence theory through high-resolution simulations. Part 1. Velocity field. *J. Fluid Mech.* **309**, 113–156.